Recruitment of Atg9 to the preautophagosomal structure by Atg11 is essential for selective autophagy in budding yeast

Congcong He,[1,3] Hui Song,[1,3] Tomohiro Yorimitsu,[1,3] Iryna Monastyrska,[1,3] Wei-Lien Yen,[1,3] Julie E. Legakis,[1,3] and Daniel J. Klionsky[1,2,3]

[1]Department of Molecular, Cellular, and Developmental Biology, [2]Department of Biological Chemistry, and [3]Life Sciences Institute, University of Michigan, Ann Arbor, MI 48109

Autophagy is a conserved degradative pathway that is induced in response to various stress and developmental conditions in eukaryotic cells. It allows the elimination of cytosolic proteins and organelles in the lysosome/vacuole. In the yeast *Saccharomyces cerevisiae*, the integral membrane protein Atg9 (autophagy-related protein 9) cycles between mitochondria and the preautophagosomal structure (PAS), the nucleating site for formation of the sequestering vesicle, suggesting a role in supplying membrane for vesicle formation and/or expansion during autophagy. To better understand the mechanisms involved in Atg9 cycling, we performed a yeast two-hybrid–based screen and identified a peripheral membrane protein, Atg11, that interacts with Atg9. We show that Atg11 governs Atg9 cycling through the PAS during specific autophagy. We also demonstrate that the integrity of the actin cytoskeleton is essential for correct targeting of Atg11 to the PAS. We propose that a pool of Atg11 mediates the anterograde transport of Atg9 to the PAS that is dependent on the actin cytoskeleton during yeast vegetative growth.

Introduction

As one of the major degradative mechanisms conserved among eukaryotic cells, autophagy mediates the turnover and recycling of long-lived cytosolic proteins and excess or damaged organelles (Klionsky, 2005). The cargo destined for autophagic degradation is sequestered in a double-membrane vesicle called an autophagosome, which fuses with the lysosome in mammalian cells or the vacuole in yeast. Eventually, the cargo is degraded by lysosomal/vacuolar resident hydrolases. Autophagy occurs in response to physiological stress or developmental signals (Levine and Klionsky, 2004). Recently, autophagy has been implicated in a variety of human diseases, including cancer, neurodegeneration, and pathogen infection (Shintani and Klionsky, 2004a). The initial identification of >20 autophagy-related (*ATG*) genes in the budding yeast *Saccharomyces cerevisiae* has highlighted this single-cell organism as a perfect model to study the molecular mechanism of autophagy, although orthologues of some yeast *ATG* genes have been found in higher eukaryotes.

Correspondence to Daniel J. Klionsky: klionsky@umich.edu

Abbreviations used in this paper: AD, activation domain; Ape1, aminopeptidase I; Atg, autophagy related; BD, binding domain; BFP, blue fluorescent protein; CC, coiled coil; Cvt, cytoplasm to vacuole targeting; PA, protein A; PAS, preautophagosomal structure; prApe1, precursor form of Ape1; SMD, synthetic minimal medium.

In yeast, autophagy can be induced under starvation conditions to reuse nutrients for essential cellular activities and proper cellular remodeling; this starvation-induced bulk autophagy is considered nonspecific. Studies in yeast have also revealed that *S. cerevisiae* has selective autophagic pathways that target specific cargos (Scott et al., 1996; Hutchins et al., 1999). These pathways mechanistically and genetically resemble bulk autophagy. One such route is the cytoplasm to vacuole targeting (Cvt) pathway (Nair and Klionsky, 2005). In this pathway, two vacuolar hydrolases, the precursor form of aminopeptidase I (Ape1 [prApe1]) and α-mannosidase, are transported to the vacuole in a double-membrane vesicle called a Cvt vesicle, with the former subsequently being processed into mature Ape1. Compared with starvation-induced autophagy, the Cvt pathway occurs constitutively in growing conditions. Although some Atg proteins appear to be pathway specific, most are involved in both the specific and nonspecific pathways. However, it is not fully understood how these proteins coordinate and function at the molecular level in either bulk or selective autophagy.

Most yeast Atg components localize at a perivacuolar punctate structure called the preautophagosomal structure (PAS) or phagophore assembly site, which is proposed to be the site of autophagosome and Cvt vesicle formation

The Journal of Cell Biology, Vol. 175, No. 6, December 18, 2006 925–935
http://www.jcb.org/cgi/doi/10.1083/jcb.200606084

(Kim et al., 2002; Noda et al., 2002). In most endomembrane trafficking systems, such as the early secretory pathway, vesicles form by budding from the surface of a preexisting organelle. However, in autophagy-related processes, the double-membrane sequestering vesicles appear to form de novo; that is, they expand by membrane addition during the formation process rather than being generated from a single piece of contiguous membrane (Reggiori and Klionsky, 2005). One of the major current challenges is to unveil where the membrane materials for autophagosomes or Cvt vesicles come from and how the lipids are transported to the assembly site. Among all Atg proteins, Atg9 is the best candidate that can help us understand this pivotal issue. Atg9 is the only characterized integral membrane protein required for both autophagosome and Cvt vesicle formation (Noda et al., 2000). However, this protein is absent from the completed vesicles, suggesting that it is retrieved before the vesicle sealing/completion step. Atg9 localizes to multiple punctate sites, with one of them corresponding to the PAS and others to mitochondria in addition to unidentified structures (Reggiori et al., 2005b). Recent studies reveal that Atg9 cycles between mitochondria and the PAS vesicle assembly site (Reggiori et al., 2004, 2005b). These characteristics make Atg9 a potential membrane carrier for vesicle formation.

We decided to investigate the molecular regulatory mechanisms underlying Atg9 cycling and, in particular, what factors regulate the anterograde transport of Atg9 to the site of vesicle formation. In this study, we discovered that a peripheral membrane protein, Atg11 (Kim et al., 2001), is an interaction partner of Atg9. The interaction requires the second coiled-coil (CC) domain of Atg11 and the Atg9 N-terminal cytosolic domain. A missense mutation (H192L) in the Atg9 N-terminal domain that disrupts its interaction with Atg11 results in the impaired cycling of Atg9 and a defect in selective autophagy. In addition, we found that in actin mutant cells, Atg11 colocalized with Atg9 and was retained on mitochondria, indicating that Atg11 is not able to direct Atg9 to the PAS in the absence of an intact cytoskeletal network. These data support a model in which a pool of Atg11 links Atg9 to the PAS along the actin cable under vegetative growth conditions.

Results

Atg11 is an interaction partner of Atg9

Atg9 is the only known transmembrane protein required for both bulk autophagy and selective autophagic processes (e.g., the Cvt pathway; Noda et al., 2000). Unlike most other Atg proteins, which are restricted to the perivacuolar PAS, Atg9 localizes to several punctate structures; one of them is at the PAS, whereas the others are primarily confined to mitochondria (Reggiori et al., 2005b). Atg9 cycles between the two compartments, suggesting that it plays a role in providing lipids to the forming autophagosomes or Cvt vesicles (Reggiori et al., 2004). However, other than actin (Reggiori et al., 2005a), the factors that regulate the anterograde transport of Atg9 to the PAS have not been identified. Therefore, we performed a yeast two-hybrid–based screen of Atg proteins to identify potential Atg9-interacting proteins. Yeast two-hybrid cells harboring Atg9 and a peripheral membrane protein, Atg11, showed robust growth on plates lacking histidine, indicating that Atg11 could interact with Atg9 (Fig. 1 A). The same result was obtained on plates lacking adenine (unpublished data).

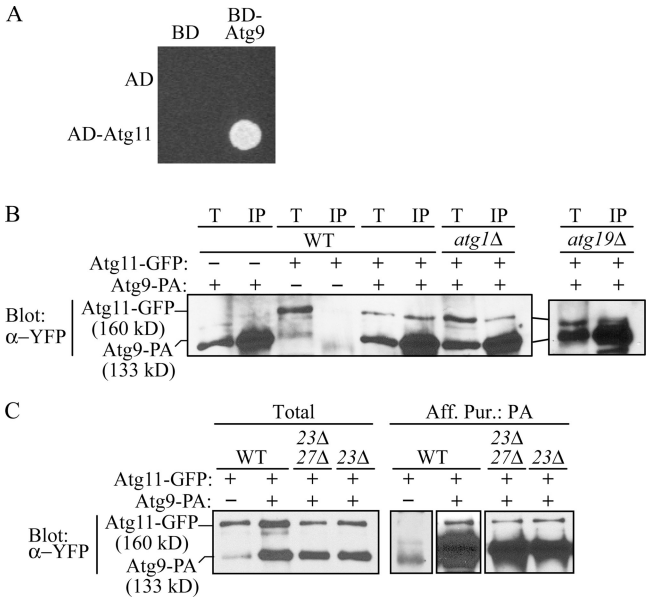

Figure 1. **Atg9 interacts with Atg11.** (A) A yeast two-hybrid assay reveals that full-length Atg9 interacts with full-length Atg11. The two-hybrid strain PJ69-4A was cotransformed with plasmids containing the activation domain (AD)–fused Atg11 and the binding domain (BD)–fused Atg9 or with empty vectors (AD and BD). Interactions were monitored by the ability of cells to grow on plates without histidine for 3 d. (B) Atg11 is coprecipitated with Atg9 independently of Atg1 and Atg19. Wild-type (TYY161), *atg1*Δ (TYY162), and *atg19*Δ (CCH005) strains expressing integrated Atg11-GFP and Atg9–protein A (PA) fusions were used for affinity isolation. Wild-type (WT) strains expressing integrated Atg9-PA alone (FRY171) or integrated Atg11-GFP (PSY101) and *CUP1* promoter-driven PA (pCuPA(414)) were used as controls. Eluted polypeptides were separated by SDS-PAGE and detected with anti-YFP antibody. The same amounts of the total lysate (T) and immunoaffinity purified isolate (IP) were loaded per gel lane. (C) Atg11 is coprecipitated with Atg9 in the absence of Atg23 and Atg27. Wild-type (TYY161), *atg23*Δ (CCH004), and *atg23*Δ *atg27*Δ (CCH006) strains expressing integrated Atg11-GFP and Atg9-PA fusions were used for affinity isolation. Total lysates and eluted polypeptides (Aff.Pur.) were separated by SDS-PAGE and visualized by immunoblotting with antibody to YFP. An Atg11-GFP strain (PSY101) expressing *CUP1*-driven PA (pCuPA(414)) alone was used as a control.

Atg11 functions in selective types of autophagy (i.e., the Cvt pathway and pexophagy) but is not essential for bulk autophagy (Kim et al., 2001). Atg11 plays a role in organizing the PAS and linking cargo to the vesicle-forming machinery at the PAS (Shintani et al., 2002; Yorimitsu and Klionsky, 2005). This protein is a component of at least two complexes in yeast. One is the Atg1–Atg11 complex, which is involved in the induction of bulk and selective autophagy (Kamada et al., 2000). The other is the Atg19–Atg11 complex, which recognizes and delivers prApe1 and α-mannosidase to the PAS (Shintani et al., 2002; Yorimitsu and Klionsky, 2005). We decided to determine whether these complexes are involved in Atg11 and Atg9 interaction. To address this issue, we used a biochemical approach to examine whether Atg11 was able to form a complex with Atg9. We tagged Atg11 with GFP and tagged Atg9 with protein A (PA) at the chromosomal locus. Wild-type, *atg1*Δ, and *atg19*Δ

cells expressing the integrated Atg9-PA and Atg11-GFP fusions were lysed, and the PA-tagged protein was isolated with IgG–Sepharose beads. Atg11 was coprecipitated with Atg9-PA in all three strains (Fig. 1 B), which verifies that these two proteins are present in a complex, although we do not know whether they interact directly. Thus, the absence of either Atg1 or Atg19 did not affect the formation of a complex between Atg9 and Atg11. This finding suggests that there might be multiple populations of Atg11 within the cell that interact with different sets of Atg proteins.

Our recent data show that two other Atg proteins, Atg23 and Atg27, interact with Atg9 and are required for Atg9 cycling. The interaction between Atg9 and either Atg23 or Atg27 is not mediated through Atg11 (Tucker et al., 2003; and unpublished data). Thus, we extended the analysis by determining whether the Atg9–Atg11 interaction was dependent on these other Atg9-interacting proteins. We found that Atg11 was coprecipitated with Atg9 in *atg23*Δ and *atg23*Δ *atg27*Δ cells despite a lower overall efficiency of recovery (Fig. 1 C). This suggests that Atg9 and Atg11 were able to form a complex in the absence of Atg23 and Atg27, although these two proteins may facilitate the interaction. The interaction between Atg9 and Atg11 in the *atg23*Δ or *atg27*Δ strains was confirmed by yeast two-hybrid analyses; the *atg23*Δ or *atg27*Δ two-hybrid cells expressing Atg9 and Atg11 were able to grow on −histidine (−His) selective plates, which is comparable with the wild-type cells (unpublished data).

Atg11 is predicted to contain four CC domains (Fig. 2 A; Yorimitsu and Klionsky, 2005). Each CC domain mediates interactions of Atg11 with different Atg proteins. To test whether these CC domains are responsible for the interaction between Atg11 and Atg9, we used CC domain deletion mutants in a series of yeast two-hybrid assays. As shown in Fig. 2 B, the two-hybrid mutant activation domain (AD)–Atg11 C-terminal truncation (11N; Δ627–1,178 and lacking CC3-4) allowed the cells to grow in the presence of binding domain (BD)–Atg9 as well as the full-length AD-Atg11. In contrast, cells expressing an AD-Atg11 N-terminal truncation (11C; Δ1–817 and lacking CC1-3) could not grow on selective −His plates (Fig. 2 B). Thus, the Atg11 N terminus is sufficient for Atg9–Atg11 interaction. In addition, Atg11ΔCC2 (Δ536–576) abolished the interaction with Atg9, whereas cells containing mutants Atg11ΔCC1 (Δ272–321), Atg11ΔCC3 (Δ627–858), or Atg11ΔCC4 (Δ859–1,178) grew well on selective plates (Fig. 2 C). These data indicated that Atg11 CC domain 2 is required for the Atg9–Atg11 interaction.

From a hydropathy plot analysis, Atg9 contains hydrophilic N and C termini flanking six to eight transmembrane domains (Noda et al., 2000). To define the topology of Atg9, we investigated the protease sensitivity of the Atg9 N and C termini. Spheroplasts derived from *pep4*Δ cells expressing either the N-terminal–tagged PA-Atg9 fusion or the C-terminal–tagged Atg9-PA fusion were osmotically lysed and centrifuged at 13,000 *g*. In agreement with previous studies, approximately two thirds of the total Atg9 was present in the S13 supernatant fraction that contained the PAS, and one third was present in the P13 pellet fraction (Fig. 2 D; Noda et al., 2000; Reggiori et al., 2005b).

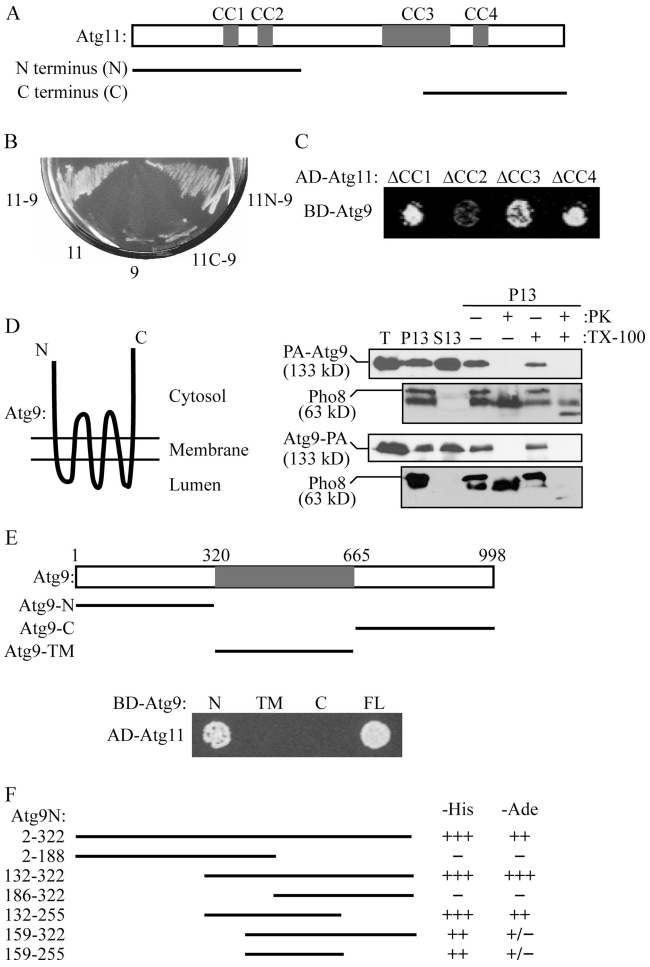

Figure 2. **The Atg9–Atg11 interaction is mediated by the Atg11 CC2 domain and the Atg9 N-terminal region.** (A) Schematic representation of Atg11 highlighting the position of the four CC domains and indicating the extent of the N- and C-terminal domains used in the two-hybrid analysis. (B) The Atg11 N terminus is sufficient to interact with Atg9 as demonstrated by the yeast two-hybrid assay. Cells expressing an Atg11 N-terminal fragment and Atg9 (11N-9), full-length Atg11 and Atg9 (11-9), the Atg11 C terminus and Atg9 (11C-9), Atg11 (11), or Atg9 (9) with the corresponding empty vector were grown for 3 d on plates lacking histidine. (C) Atg11 CC domain 2 is essential for Atg11–Atg9 interaction. Cells expressing Atg9 and Atg11 lacking the indicated coiled-coil (CC) domains were grown for 3 d on −His plates. (D) Both the N and C termini of Atg9 are protease sensitive. A schematic representation of Atg9 topology is shown on the left. *pep4*Δ cells expressing either integrated C-terminally tagged Atg9-PA (FRY172) or *CUP1*-driven N-terminally tagged PA-Atg9 (TVY1; pCuPAAtg9(416)) were converted to spheroplasts and osmotically lysed, and the pellet fraction was subjected to proteinase K (PK) treatment in the presence or absence of Triton X-100 (TX-100). Fractions were analyzed by immunoblotting with antibodies to PA and Pho8. T, total. (E) The Atg9 N terminus interacts with Atg11. A schematic diagram of Atg9 and domains used for two-hybrid analysis are depicted. Cells expressing Atg11 and the Atg9 N-terminal fragment (N), transmembrane domain (TM), C terminus (C), or full-length Atg9 (FL) were grown for 3 d on −His plates. (F) Atg9 N-terminal amino acids 159–255 are the minimal sufficient region needed to interact with Atg11. A truncation series of the Atg9 N-terminal region in the binding domain (BD) two-hybrid plasmid is depicted. The strength of the corresponding proteins to interact with activation domain (AD)–Atg11 is indicated on the right by the robustness of cell growth on plates without histidine (−His) or adenine (−Ade) for 5 d.

When the P13 fraction was treated with exogenous proteinase K, both the N- and C-terminal PA tags were cleaved in the absence or presence of detergent, and no bands of smaller molecular mass were detected (Fig. 2 D), indicating that both the N and C termini of Atg9 were accessible to protease on the cytosolic side of the membrane. To verify that intracellular membranous structures were intact after osmotic lysis, we simultaneously monitored the protease sensitivity of an endogenous vacuole membrane protein, Pho8. The precursor form of Pho8 that accumulated in the *pep4Δ* background contains a small cytosolic tail and a lumenally oriented propeptide (Fig. 2 D). In the absence of detergent, only the Pho8 cytosolic tail but not the lumenal propeptide was accessible to proteinase K. Upon the addition of both detergent and proteinase K, the Pho8 lumenal propeptide was removed as a result of the disruption of all membranous compartments, which is shown as a further shift of the molecular mass (Fig. 2 D). Thus, these data verified the integrity of the relatively fragile vacuole and presumably other intracellular membranous compartments after osmotic lysis, suggesting that both the N and C termini of Atg9 are exposed to the cytosol (Fig. 2 D). Accordingly, the topology of Atg9 appears to be conserved between yeast and mammalian cells (Young et al., 2006).

So far, no known functional domains have been identified in the Atg9 N- or C- terminal regions. To further analyze the Atg9–Atg11 interaction, we generated truncated Atg9 mutants containing the N terminus, C terminus, or transmembrane region. As shown in Fig. 2 E, in the presence of Atg11, the Atg9 N-terminal domain supported the growth of two-hybrid cells as well as the full-length Atg9, whereas neither the C-terminal nor the transmembrane domains of Atg9 were able to do so (Fig. 2 E). This result showed that Atg11 interacts with the N-terminal region of Atg9. We further constructed a series of Atg9 N-terminal truncation mutants and analyzed them for interaction with Atg11 by yeast two-hybrid analysis. Atg9 N-terminal amino acids 159–255 appeared to be the minimal region that mediates the interaction with Atg11 (Fig. 2 F). Collectively, we concluded that Atg11 and Atg9 interact through the Atg11 CC domain 2 and the Atg9 N terminus.

Atg11 recruits Atg9 to the PAS

In wild-type cells, Atg11 localizes at the PAS (Kim et al., 2001), and Atg9 cycles between the PAS and mitochondria (Reggiori et al., 2004, 2005b). To examine the role of the interaction between Atg9 and Atg11, we analyzed the cycling of Atg9 in the presence of overexpressed Atg11 or in the absence of this protein. The chromosomally tagged Atg9-YFP chimera displayed a multiple punctate distribution in wild-type cells, with one of the puncta colocalizing with the PAS marker blue fluorescent protein (BFP)–Ape1 (Fig. 3 A). In contrast, in the *atg1Δ* background, Atg9 was restricted to the PAS, which is in agreement with previous observations that indicated a role for Atg1 in the retrograde transport of Atg9 from the PAS to mitochondria (Reggiori et al., 2004, 2005a,b). In 91% (109/120) of the cells overexpressing Atg11, Atg9-YFP localized solely to the perivacuolar PAS (represented by CFP-Atg11), which is similar to the situation observed in *atg1Δ* cells (Fig. 3 A; Kim et al., 2002),

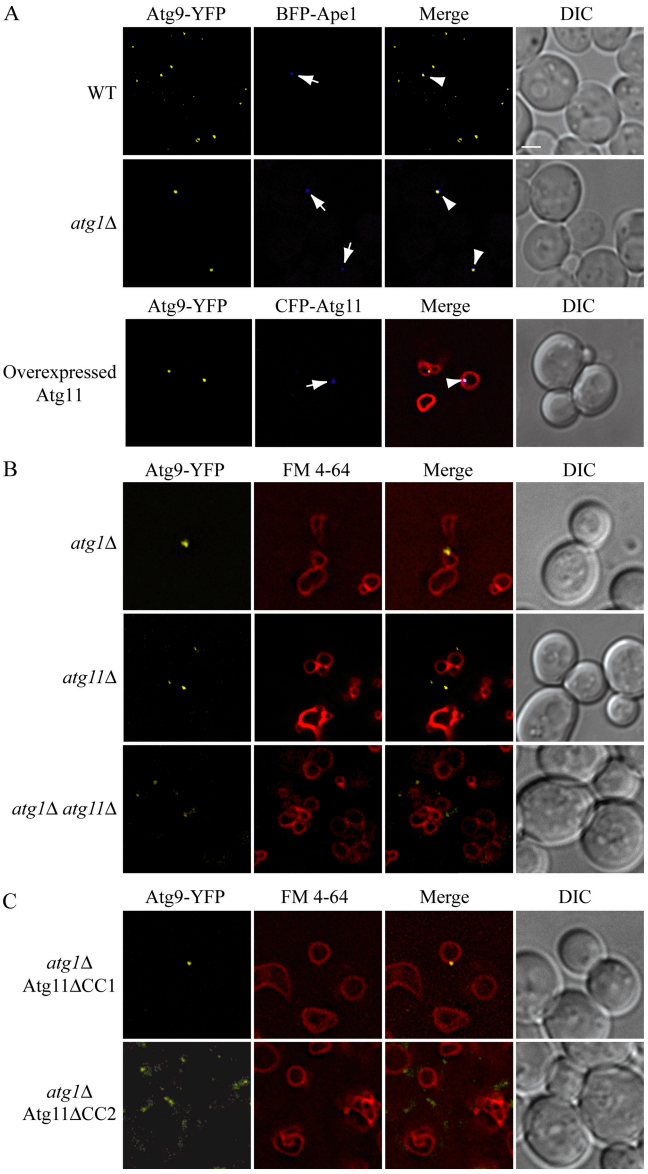

Figure 3. **Atg9 cycles through the PAS in an Atg11-dependent manner.** (A) Atg11 overexpression restricts Atg9 to the PAS. Wild-type (WT) or *atg1Δ* strains expressing an integrated Atg9-YFP fusion (FRY136 and FRY138, respectively) were transformed with a plasmid containing BFP-Ape1 (pBFPApe1(414)) as the PAS marker. In addition, an *atg11Δ* strain (KTY53) expressing an integrated Atg9-YFP fusion was transformed with a centromeric plasmid containing *CUP1* promoter-driven CFP-Atg11 (pCuHACFPCVT9(414)). Cells were grown to mid-log phase and visualized by fluorescence microscopy. Arrows mark the PAS localization of BFP-Ape1, and arrowheads mark the sites of colocalization. (B) Atg9 fails to transport to the PAS in mutants deleted for Atg11. *atg1Δ* (FRY138), *atg11Δ* (KTY53), or *atg1Δ atg11Δ* (YTS150) strains expressing chromosomally tagged Atg9-YFP were imaged by fluorescence microscopy. (C) The second Atg11 CC domain is needed for correct Atg9 cycling. The *atg1Δ atg11Δ* strain (YTS150) was transformed with a plasmid encoding the Atg11ΔCC1 or Atg11ΔCC2 mutants, and YFP fluorescence was visualized by fluorescence microscopy. In all panels, cells were stained with FM 4-64 to label the vacuole before being imaged by fluorescence microscopy. DIC, differential interference contrast. Bar, 2 μm.

and did not localize to mitochondria (not depicted). Thus, excess Atg11 was able to restrict Atg9 to the PAS. Overexpressed Atg11 displays a dominant-negative phenotype, interfering with

the vacuolar import of prApe1 through the Cvt pathway (unpublished data). The dominant-negative phenotype presumably reflects the defect in Atg9 cycling.

To further examine the role of Atg11 in recruiting Atg9 to the PAS, we used the TAKA (transport of Atg9 after knocking out *ATG1*) assay (Cheong et al., 2005). This assay examines the epistasis of a second mutation relative to *atg1*Δ with regard to Atg9 localization at the PAS. We visualized chromosomally tagged Atg9-YFP in *atg11*Δ single and *atg1*Δ *atg11*Δ double deletion cells and simultaneously labeled the vacuolar membrane with FM 4-64. As shown previously, in *atg1*Δ cells, Atg9-YFP localized to a single perivacuolar punctum, which corresponds to the PAS (Fig. 3 B). In contrast, in nearly 90% of the *atg11*Δ or *atg1*Δ *atg11*Δ mutants, Atg9-YFP fluorescence showed multiple puncta and did not localize at a single perivacuolar structure, suggesting that its anterograde transport was blocked because of the *ATG11* deletion (Fig. 3 B). These results suggest that Atg11 is involved in the anterograde transport of Atg9.

Our mapping of the Atg9 and Atg11 interaction domains indicated that Atg11ΔCC2 but not Atg11 lacking its other CC domains was defective in forming a complex with Atg9 (Fig. 2). Accordingly, we examined the effect of Atg11 CC deletions on Atg9 subcellular distribution. As shown in Fig. 3 C, in cells expressing Atg11ΔCC1 in the *atg1*Δ background, Atg9 localized to the PAS, which is similar to the result seen in *atg1*Δ cells expressing wild-type Atg11. In contrast, in cells expressing Atg11ΔCC2, which lacks the Atg9-interacting domain, Atg9 displayed a multiple punctate distribution (Fig. 3 C) resembling that observed in *atg1*Δ *atg11*Δ cells even though the mutant protein was expressed at a level similar to the wild-type protein (Yorimitsu and Klionsky, 2005). Thus, we concluded that the interaction of Atg9 with Atg11 CC domain 2 is required to direct Atg9 to the PAS.

The Atg9^{H192L} mutant is defective for the Cvt pathway

To further clarify the physiological functions of the Atg9–Atg11 interaction, we decided to test whether autophagic processes were affected by its disruption. It has been reported that Atg11 CC domain 2, the Atg9-interacting domain, interacts with multiple Atg proteins, including at least one (Atg1) that is involved in Atg9 retrograde transport (Yorimitsu and Klionsky, 2005). Thus, Atg11ΔCC2 may cause pleiotropic effects when used in functional studies. To bypass this problem, we decided to use native Atg11 and instead to isolate mutations within the Atg9 N-terminal region that disrupt the interaction with Atg11. We performed a PCR-based random mutagenesis on the N-terminal region of Atg9 followed by a yeast two-hybrid screen for loss-of-interaction mutants. A missense mutation was identified with a single histidine to leucine substitution at position 192 (H192L), which is located in the minimal region (amino acids 159–255) needed for the Atg9–Atg11 interaction (Fig. 2 E). Two-hybrid cells harboring this mutation completely lost the capacity for growth on selective −adenine (−Ade) plates in the presence of Atg11 (Fig. 4 A), whereas the expression level of the mutant protein was comparable with that of the wild type (not depicted).

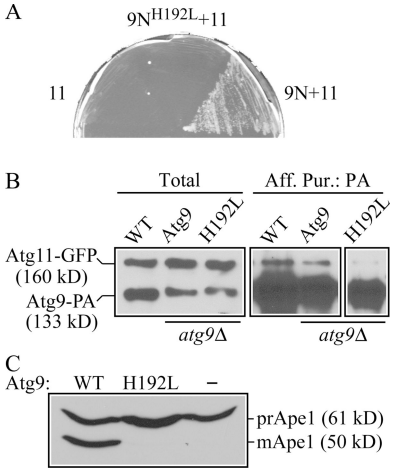

Figure 4. **The Atg9^{H192L} mutant is defective for the Cvt pathway.** (A) The Atg9 H192L mutation disrupts the interaction between Atg9 and Atg11 by yeast two-hybrid assay. Cells expressing Atg11 (AD-Atg11) and either the empty plasmid (11), the Atg9 N terminus harboring the H192L mutation (BD–Atg9N^{H192L}; 9N^{H192L}+11), or the wild-type Atg9 N-terminal fragment (9N+11) were grown for 5 d on −Ade plates. (B) Atg11 is coprecipitated with wild-type Atg9 but not with Atg9^{H192L}. An *atg9*Δ strain expressing an integrated Atg11-GFP fusion (CCH007) was transformed with a plasmid expressing either wild-type Atg9-PA (pAtg9PA(314); Atg9) or Atg9^{H192L}-PA (pAtg9^{H192L}PA(314); H192L) driven by the Atg9 native promoter. The affinity isolation was performed as described in Materials and methods. Eluted polypeptides were separated by SDS-PAGE and detected with anti-YFP antibody. A wild-type strain expressing integrated Atg11-GFP and Atg9-PA fusions (TYY161) was used as a control (WT). (C) Precursor Ape1 maturation is blocked in cells expressing Atg9^{H192L}. The *atg9*Δ strain (JKY007) was transformed with a plasmid expressing wild-type Atg9 (pAPG-9GFP(416)), Atg9^{H192L} (pAtg9^{H192L}GFP416; H192L), or an empty vector (pRS416; −). Cells were grown to mid-log phase, and protein extracts were analyzed by Western blotting using antiserum to Ape1. The positions of precursor and mature Ape1 are indicated.

This indicates that the interaction between Atg9 and Atg11 was abolished by the H192L mutation. The loss of Atg9–Atg11 interaction was confirmed by a coimmunoprecipitation assay. As shown in Fig. 4 B, endogenous Atg11 was recovered only with wild-type Atg9 but not with the Atg9^{H192L} mutant. In contrast, yeast two-hybrid data indicated that the interaction between Atg9 and either Atg2 or Atg18, two proteins involved in the retrograde transport of Atg9, was unaffected (unpublished data).

Because both *ATG9* and *ATG11* are essential genes for the Cvt pathway, which is a type of selective autophagy, we monitored the processing of prApe1 as a marker protein for this transport route. As shown in Fig. 4 C, cells expressing Atg9^{H192L} did not generate the mature form of Ape1 compared with cells expressing wild-type Atg9, indicating that the Cvt pathway was impaired by the Atg9 H192L mutation.

Anterograde movement of Atg9^{H192L} is blocked in growing conditions

We were interested in determining whether the impairment of the Cvt pathway seen with Atg9^{H192L} (Fig. 4 B) was caused by defects in Atg9 cycling, particularly anterograde movement to the PAS. Accordingly, we used the TAKA assay to visualize the cycling of Atg9^{H192L}-GFP in growing conditions and concurrently stained mitochondria with the dye MitoFluor red. In the *atg1*Δ background, wild-type Atg9-GFP was restricted to the

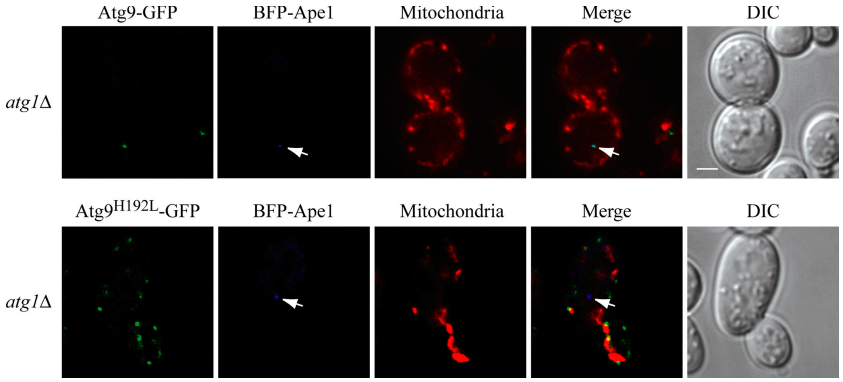

Figure 5. **Anterograde transport of Atg9 to the PAS is impaired in the Atg9^{H192L} mutant under growing conditions.** The *atg1*Δ *atg9*Δ strain (CCH001) was cotransformed with a BFP-Ape1 plasmid (pBFPApe1(414)) and a plasmid expressing wild-type Atg9-GFP (pAPG9GFP(416)) or Atg9^{H192L}-GFP (pAtg9^{H192L}GFP(416)). Cells were cultured to mid-log phase and stained with MitoFluor red 589 as described in Materials and methods before imaging by fluorescence microscopy. Arrows mark the locations of BFP-Ape1. DIC, differential interference contrast. Bar, 2 μm.

PAS, as marked with BFP-Ape1 in 94% (116/123) of the cells examined (Fig. 5). In contrast, Atg9^{H192L}-GFP distributed to multiple punctate structures in 84% (131/156) of the *atg1*Δ cells, which colocalized, in part, with the mitochondrial labeling but not with the PAS. Thus, the Atg9^{H192L} mutation acted epistatically to *atg1*Δ, suggesting that the anterograde movement of Atg9^{H192L} from mitochondria to the PAS was defective.

Bulk autophagy is not affected by disruption of the Atg9–Atg11 interaction

Atg9 is essential for both bulk autophagy and the Cvt pathway, whereas Atg11 is required solely in the Cvt pathway (Noda et al., 2000; Kim et al., 2001). To clarify whether Atg9 anterograde transport via Atg11 is involved in bulk autophagy, we used the Atg9^{H192L} mutant to analyze the progression of bulk autophagy by several established assays.

Atg8 conjugated to phosphatidylethanolamine remains associated with the completed autophagosome and is a marker for autophagic delivery to the vacuole (Kirisako et al., 1999, 2000; Huang et al., 2000). After delivery of the GFP-tagged Atg8 chimera, the GFP moiety is cleaved and remains relatively stable in the vacuole, whereas Atg8 is rapidly degraded. Thus, the accumulation of free GFP reflects the progression of bulk autophagy, which can be readily detected by Western blotting (Shintani and Klionsky, 2004b; Cheong et al., 2005). In *atg9*Δ cells, essentially no free GFP was detected, indicating that bulk autophagy was blocked by *ATG9* deletion (Fig. 6 A). In cells expressing wild-type Atg9 or Atg9^{H192L}, free GFP was detectable starting 2 h after cells were shifted to starvation conditions (synthetic medium lacking nitrogen [SD-N]) to induce bulk autophagy, although GFP-Atg8 processing showed a delay in Atg9^{H192L} cells compared with wild-type cells. This result demonstrated that bulk autophagy retained similar activity even when Atg9 failed to interact with the Cvt-specific component Atg11.

To confirm the aforementioned result, we quantitatively measured bulk autophagy activity using another marker protein, Pho8Δ60, which encodes an altered form of alkaline phosphatase that is only delivered to the vacuole via autophagy (Noda et al., 1995). The Pho8Δ60 enzymatic activity was measured in wild-type and *atg1*Δ cells and in *atg9*Δ cells transformed with a plasmid expressing wild-type Atg9 or Atg9^{H192L} or an empty vector in growing (synthetic minimal medium [SMD]) and starvation (SD-N) conditions (Fig. 6 B). The *atg1*Δ or *atg9*Δ cells transformed with an empty vector showed only the basal level of Pho8Δ60 activity after autophagy induction (SD-N), indicating that bulk autophagy was defective after deleting either gene. In contrast, there was an increase of Pho8Δ60 activity in *atg9*Δ cells expressing either wild-type Atg9 or Atg9^{H192L}, indicating that Atg9^{H192L} rescued the autophagy defect in *atg9*Δ cells, which is comparable with the wild-type Atg9 protein. Collectively, these data suggested that bulk autophagy does not depend on the interaction between Atg9 and an Atg protein that is needed for anterograde movement during specific autophagy (Atg11).

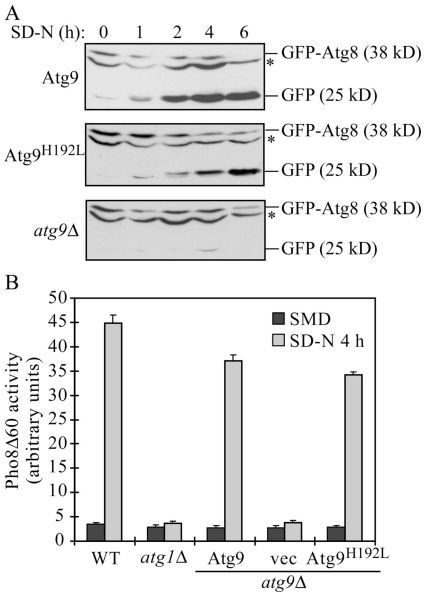

Figure 6. **Bulk autophagy is normal with the Atg9^{H192L} mutant.** (A) GFP-Atg8 processing is not affected by Atg9^{H192L}. The *atg9*Δ strain (JKY007) was cotransformed with a GFP-Atg8 plasmid (pGFPAUT7(414)) and a plasmid expressing wild-type Atg9 (pAPG9GFP(416)), Atg9^{H192L} (pAtg9^{H192L}GFP(416)), or an empty vector (pRS416; *atg9*Δ). Cells were grown in SMD to mid-log phase and shifted to starvation conditions (SD-N). At the indicated time points, aliquots were taken, and protein extracts were analyzed by Western blotting using anti-GFP antibody. The positions of GFP-Atg8 and free GFP are indicated. The asterisks mark nonspecific bands. (B) Pho8Δ60 activity is normal in Atg9^{H192L}-expressing cells. The wild-type (WT; YTS158) and *atg1*Δ (TYY127) strains and the *atg9*Δ strain (CCH002) transformed with a plasmid expressing wild-type Atg9 (pAPG9(416)), Atg9^{H192L} (pAtg9^{H192L}(416)), or an empty vector (pRS416;vec) were grown in SMD to mid-log phase and shifted to SD-N for 4 h. The Pho8Δ60 activity was measured as described in Materials and methods. Error bars indicate the SEM of three independent experiments.

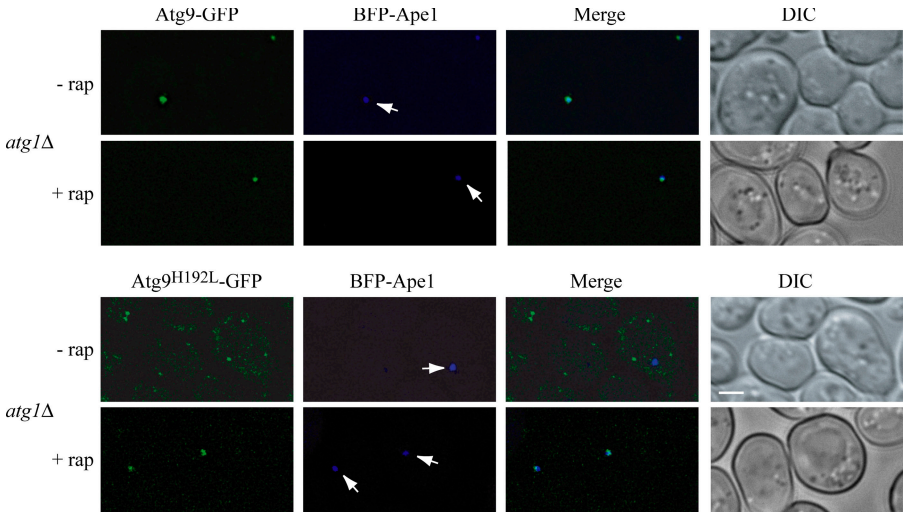

Figure 7. **Anterograde transport of Atg9^{H192L} is normal upon bulk autophagy induction.** The *atg1*Δ *atg9*Δ strain (CCH001) was cotransformed with a BFP-Ape1 plasmid (pBFPApe1(414)) and a plasmid expressing wild-type Atg9-GFP (pAPG9GFP(416)) or Atg9^{H192L}-GFP (pAtg9^{H192L}GFP(416)). Bulk autophagy was induced by rapamycin treatment (+rap) as described in Materials and methods before imaging by fluorescence microscopy. Arrows mark the PAS localization of BFP-Ape1. DIC, differential interference contrast. Bar, 2 μm.

Atg9^{H192L} cycling is normal during bulk autophagy

Because bulk autophagy activity was not affected by the Atg9 H192L mutation, it was tempting to speculate that Atg9^{H192L} cycled normally under starvation conditions even though it was not capable of forming a complex with Atg11. To test this hypothesis, we visualized the movement of Atg9^{H192L} by the TAKA assay after autophagy induction. Cells were treated with the drug rapamycin, which mimics starvation conditions and induces bulk autophagy. As shown in Fig. 7, in the *atg1*Δ background without rapamycin treatment (−rap), wild-type Atg9-GFP was restricted to the PAS, whereas Atg9^{H192L}-GFP could not move to the PAS and displayed a multiple punctate localization. After treatment with rapamycin (Fig. 7, +rap), in 85% (41/48) of the cells, Atg9^{H192L}-GFP colocalized with the PAS marker BFP-Ape1 similarly to wild-type Atg9, indicating that Atg9 recruitment to the PAS was normal. Therefore, this result demonstrated that during bulk autophagy, the Atg9^{H192L} mutation did not interfere with the cycling of Atg9.

Atg11 localization to the PAS is dependent on the actin cytoskeleton

Recently, we have shown that Atg9 anterograde traffic to the PAS is blocked when the actin cytoskeleton is disrupted by either treatment with the drug latrunculin A or point mutations in *ACT1*, the gene encoding actin (Reggiori et al., 2005a). In particular, the impairment of actin function leads to a defect in the Cvt pathway, whereas bulk autophagy is normal; a similar phenotype was also observed with the Atg9^{H192L} mutant. Because Atg9 anterograde transport was also dependent on its interaction with Atg11 (Fig. 3), we wondered whether there was a functional connection between actin and Atg11 in Atg9 cycling and autophagic processes. Previous data show that Atg11 is needed to recruit prApe1 to the PAS (Yorimitsu and Klionsky, 2005). The *atg9*-null mutant does not affect the recruitment of prApe1 to the PAS or the localization of Atg11 (unpublished data), suggesting that Atg11 localization at the PAS is not dependent on the Atg9–Atg11 interaction. Thus, we propose that Atg11 mediates actin-dependent Atg9 cycling in the Cvt pathway.

To test this hypothesis, we used an actin mutant, *act1-159*, which has defects in actin cable depolymerization, Atg9 cycling, and the Cvt pathway (Reggiori et al., 2005a). As shown in Fig. 8 A, in wild-type cells, GFP-Atg11 localized to the PAS as a single punctum; chromosomally tagged Atg9-RFP displayed a multiple punctate localization pattern. In the *act1-159* mutant, however, GFP-Atg11 redistributed to cytoplasmic patches, which partially colocalized with Atg9-RFP. To reveal the identity of these multiple compartments, we stained cells with the mitochondrial dye MitoFluor red and the vacuolar membrane dye FM 4-64. As shown in Fig. 8 B, in 81% (81/100) of the cells, the GFP-Atg11 patches were absent from the perivacuolar PAS position; instead, they colocalized with the mitochondrial labeling, indicating that Atg11 localized at mitochondria when the actin network was defective. Therefore, the proper localization of Atg11 to the PAS is dependent on the actin cytoskeleton and may underlie the actin-dependent Atg9 cycling during the Cvt pathway and other types of specific autophagy.

Discussion

Atg9 is the only characterized transmembrane protein involved in the formation of the sequestering vesicles that form during the Cvt pathway, pexophagy, and autophagy. Accordingly, it is the best candidate to mark the source of the vesicle membrane. Recently, we have shown that Atg9 localizes to mitochondria in addition to the PAS, implicating this organelle in supplying membrane during autophagy-related processes (Reggiori et al., 2005b). Only Atg19, which is a receptor for biosynthetic cargos, and Atg8 remain associated with the completed vesicles; most of the soluble Atg proteins involved in vesicle formation presumably dissociate from the membrane before or upon vesicle completion. In contrast, a specific retrieval mechanism operates in the cycling of Atg9 and the associated protein Atg23 (Reggiori et al., 2004). The retrograde movement of Atg9 from the PAS to mitochondria requires Atg1–Atg13, Atg2, Atg18, and the PtdIns3–kinase complex. The transit of Atg9 to the PAS involves Atg23, Atg27, and actin (Reggiori et al., 2005a;

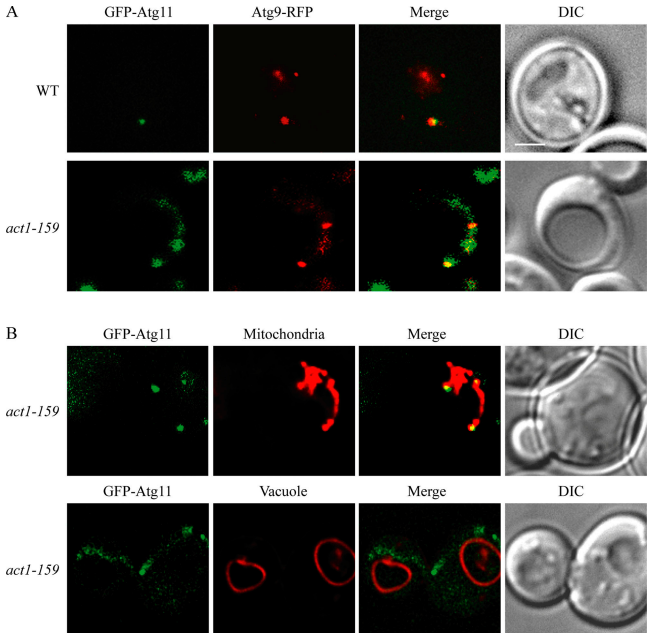

Figure 8. **Atg11 localization at the PAS is dependent on the actin cytoskeleton.** (A) Atg11 alters its distribution in the *act1-159* mutant and colocalizes with Atg9. Wild-type (WT; FRY245) and *act1-159* (IRA004) strains expressing an integrated Atg9-RFP fusion were transformed with a plasmid containing GFP-Atg11 (pTS495). Cells were grown to mid-log phase at 30°C and imaged by fluorescence microscopy. (B) Atg11 is localized to mitochondria in the *act1-159* mutant. The *act1-159* (IRA004) strain was transformed with the GFP-Atg11 plasmid. Cells were treated with MitoFluor red 589 or FM 4-64 as described in Materials and methods and were imaged by fluorescence microscopy. DIC, differential interference contrast. Bar, 1 µm.

Yen et al., 2006; and unpublished data); however, the mechanism by which actin mediates Atg9 movement is not known.

To identify other Atg components involved in the anterograde movement of Atg9, we performed a yeast two-hybrid screen for proteins that interact with Atg9 and identified Atg11 (Fig. 1). This result is intriguing because Atg11 has previously been shown to interact with Atg19 and Atg1, which are components involved in distinct steps of a specific autophagic process. In conjunction with the present result, we propose that Atg11 acts as a scaffold to coordinate the delivery of multiple components, including the cargo–receptor complex, components involved in vesicle formation, and proteins involved in supplying membrane, to the site of vesicle formation, the PAS (Fig. 9). The Atg11 CC domain2 interacts with the N terminus of Atg9 (Fig. 2), and the interaction occurs in the absence of Atg1 or Atg19 (Fig. 1), suggesting that there are distinct and multiple populations of Atg11 within the cell. Atg11 self-interaction (Yorimitsu and Klionsky, 2005) may then allow these various populations of Atg proteins to be delivered to the PAS in a coordinated manner. Consistent with this model, the overexpression of Atg11 restricted Atg9 to the PAS, presumably as a result of enhanced delivery (Fig. 3). In contrast, a mutation of H192L that disrupts interaction between Atg9 and the specific autophagy component Atg11 resulted in a defect in transporting Atg9 to the PAS (Fig. 5). Furthermore, the absence of Atg9 at the PAS caused by this point mutation led to a block in the Cvt pathway (Fig. 4).

It is known that Atg11 is needed for specific types of autophagy such as the Cvt pathway but is not essential for nonspecific autophagy (Kim et al., 2001). We found that the Atg9 point mutant that disrupts the interaction with Atg11 imposed little effect on the bulk autophagy induced during starvation (Fig. 6). The essentially normal autophagy function was correlated with the normal localization/transport of the binding-defective Atg9 mutant in the presence of the autophagy inducer rapamycin (Fig. 7). This finding suggests that the anterograde transport of Atg9 during bulk autophagy may be mediated by a different mechanism that is at least relatively independent of Atg11. Thus, other proteins that may interact with Atg9 deserve further investigation to reveal the Atg9 cycling machinery that operates during bulk autophagy; however, we cannot rule out the possibility that a low level of interaction between $Atg9^{H192L}$ and Atg11 allows the anterograde transport of $Atg9^{H192L}$ after autophagy induction.

Finally, we found that actin is required for the localization of Atg11 to the PAS (Fig. 8). This observation, coupled with the role of Atg11 in Atg9 anterograde movement but not vice versa, suggests that Atg11 mediates the connection between actin and Atg9 delivery from the mitochondria to the PAS. Actin is not needed for bulk autophagy in yeast (Reggiori et al., 2005a), which is in agreement with our findings in the present paper that the $Atg9^{H192L}$ mutant is not defective for nonspecific autophagy. It is not known how Atg9 might move along actin cables. The third Atg11 CC domain displays some similarity with that of

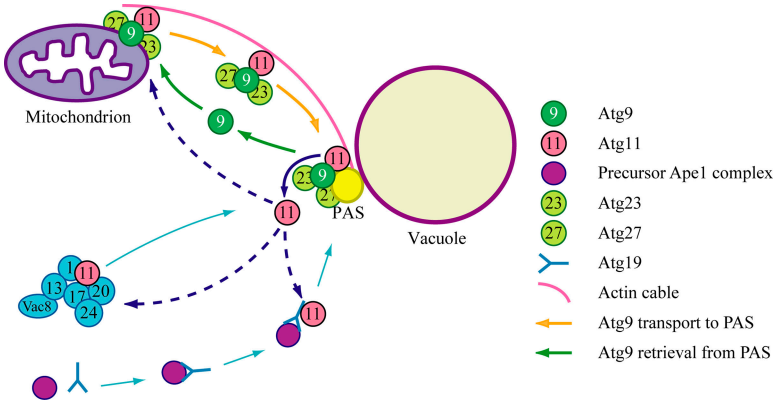

Figure 9. **Model of Atg9 transport mediated by Atg11.** The transmembrane protein Atg9 cycles between the PAS and mitochondria. The potential role of Atg9 cycling is to provide lipids for vesicle formation in bulk and selective autophagy. In the latter, a pool of the peripheral membrane protein Atg11 along with Atg23 and Atg27 (Reggiori et al., 2005a; Yen et al., 2006; and unpublished data) regulates the anterograde movement of Atg9 from mitochondria to the PAS, which is dependent on actin function. The other two known Atg11 populations in yeast are indicated: the Atg1–Atg11 complex (consisting of Atg1, Atg11, Atg13, Atg17, Atg20, Atg24, and Vac8) and the Atg11–Atg19 complex (consisting of prApe1, the prApe1 receptor Atg19, and Atg11). The retrieval of Atg9 requires the Atg1–Atg13 complex, Atg2, Atg18, and the PtdIns3–kinase complex (not depicted).

Myo2; however, Atg11 lacks the N-terminal motor domain that functions in Myo2 movement (Monastyrska et al., 2006). Thus, it is not clear how Atg11 might actually mediate the anterograde movement of Atg9. Continued analysis of Atg9 cycling and its interactions with Atg11 and other Atg proteins may provide insight into the underlying mechanisms of membrane delivery during Cvt vesicle and autophagosome formation.

Materials and methods

Strains, plasmids, and media

The *S. cerevisiae* strains used in this study are listed in Table I. For gene disruption, the entire coding region was replaced by the *S. cerevisiae TRP1*, the *Kluyveromyces lactis LEU2* or *URA3*, the *Saccharomyces kluyveri HIS3*, or the *Escherichia coli kan*^{r} gene using PCR primers containing ~50 bases of identity to the regions flanking the open reading frame. For PCR-based integrations of the PA and GFP tags at the 3′ end of the *ATG9* and *ATG11* genes, pHAB102 and pFA6a-GFP-HIS3 were used as templates to generate strains expressing fusion proteins under the control of their native promoters (Longtine et al., 1998; Abeliovich et al., 2003).

Yeast cells were grown in rich medium (YPD; 1% yeast extract, 2% peptone, and 2% glucose) or SMD (0.67% yeast nitrogen base, 2% glucose, amino acids, and vitamins as needed). Starvation experiments were conducted in SD-N (0.17% yeast nitrogen base without amino acids and 2% glucose).

Plasmids expressing Atg11 truncations (Yorimitsu and Klionsky, 2005), GFP-Atg8 (pGFP-AUT7(414); Abeliovich et al., 2003), Atg9 (pAPG9(416); essentially constructed the same as pAPG9(414); Noda et al., 2000), Atg9-GFP (pAPG9GFP(416); Noda et al., 2000), and CFP-Atg11 (pCuHACFPCVT9(414); Kim et al., 2002) have been described previously. BFP-Ape1 (pBFPApe1(414)) was constructed by introducing BFP (Qbiogene) on a BamHI PCR-generated fragment into a unique BglII site situated after the start codon of *APE1* (Shintani et al., 2002). GFP-Atg11 (pTS495) was constructed in a similar manner starting with *ATG11* cloned into the pRS416 vector. PA-Atg9 (pCuPAAtg9(416)) was generated by cloning *ATG9* into the pRS416-CuProtA vector (Kim et al., 2002). Full-length Atg9 (pBD-Atg9) and the Atg9 N-terminal (pBD-Atg9N), C-terminal (pBD-Atg9C), and transmembrane (pBD-Atg9TM) regions were amplified by PCR from pAPG9(416) and introduced into the two-hybrid vector pGBDU-C1 using BamHI and SalI sites. A total of 19 other *ATG* genes were amplified and cloned into the two-hybrid vector pGAD-C1 using BamHI and SalI sites. The serial deletion mutants of the Atg9 N terminus were generated by PCR amplification from pBD-Atg9N and ligated into the EcoRI and BamHI sites of pGBDU-C1. The plasmid expressing the Atg9^{H192L} mutant (pAtg9^{H192L}(416)) was constructed by releasing the *ATG9* fragment containing H192L from pAtg9^{H192L}GFP(416) (see Random mutagenesis screen…mutant) and was cloned into pAPG9(416) using SacI and AgeI. pAtg9PA(314) and pAtg9^{H192L}PA(314) were constructed by PCR amplifying *ATG9* and *ATG9*^{H192L} together with its native promoter from pAPG-9GFP(416) and pAtg9^{H192L}GFP(416) and incorporating them into pNopPA(314) using XhoI and XmaI sites. pNopPA(314) was a gift from F. Reggiori (University of Utrecht, Utrecht, Netherlands).

PA affinity isolation

Cells were grown to OD_{600} = 0.8 in SMD, and 100 ml were harvested and resuspended in lysis buffer (PBS, 200 mM sorbitol, 1 mM $MgCl_2$, 0.1% Tween 20, 1 mM PMSF, and protease inhibitor cocktail). The detergent extracts were incubated with IgG–Sepharose beads overnight at 4°C. The beads were washed with lysis buffer eight times and eluted in SDS-PAGE sample buffer by incubating at 55°C for 15 min. The eluates were resolved by SDS-PAGE and immunoblotted with anti-YFP antibody.

Random mutagenesis screen and generation of the Atg9 mutant

The gap repair PCR mutagenesis method (Oda et al., 1996) was used to generate the Atg11 binding–defective Atg9 mutant. An AvrII site at 942 bp

Table I. **Yeast strains used in this study**

Strain	Genotype	Reference
BY4742	*MATα ura3Δ leu2Δ his3Δ lys2Δ*	Invitrogen
CCH001	SEY6210 *atg9Δ::HIS5 atg1Δ::LEU2*	This study
CCH002	YTS158 *atg9Δ::HIS5*	This study
CCH004	TYY161 *atg23Δ::URA3*	This study
CCH005	TYY161 *atg19Δ::URA3*	This study
CCH006	TYY161 *atg23Δ::URA3 atg27Δ::LEU2*	This study
CCH007	PSY101 *atg9Δ::LEU2*	This study
DDY1493	*MATα ura3-52 leu2-3,112 his3-Δ200 tub2-201 act1-159::HIS3*	Drubin et al., 1993
FRY136	SEY6210 *ATG9-YFP::HIS3*	Cheong et al., 2005
FRY138	SEY6210 *ATG9-YFP::HIS3 atg1Δ::URA3*	Reggiori et al., 2004
FRY171	SEY6210 *ATG9-PA::TRP1*	This study
FRY172	SEY6210 *ATG9-PA::TRP1 pep4Δ::LEU2*	Reggiori et al., 2004
FRY245	SEY6210 *ATG9-RFP::HIS3*	Reggiori et al., 2005b
IRA004	DDY1493 *ATG9-RFP::KAN*	Reggiori et al., 2005b
JKY007	SEY6210 *atg9Δ::HIS3*	Noda et al., 2000
JLY87	PJ69-4A *atg23Δ::KAN* J.	Unpublished data
JLY88	PJ69-4A *atg27Δ::KAN*	Unpublished data
KTY53	SEY6210 *ATG9-YFP::HIS3 atg11Δ::URA3*	Reggiori et al., 2004
PJ69-4A	*MATα leu2-3,112 trp1-Δ901 ura3-52 his3-Δ200 gal4Δ gal80Δ LYS2::GAL1-HIS3 GAL2-ADE2 met2::GAL7-lacZ*	James et al., 1996
PSY101	SEY6210 *ATG11-GFP::HIS3*	This study
SEY6210	*MATα ura3-52 leu2-3,112 his3-Δ200 trp1-Δ901 lys2-801 suc2-Δ9 mel GAL*	Robinson et al., 1988
TVY1	SEY6210 *pep4Δ::LEU2*	Gerhardt et al., 1998
TYY127	YTS158 *atg1Δ::HIS5*	This study
TYY161	SEY6210 *ATG11-GFP::HIS3 ATG9-PA::TRP1*	This study
TYY162	TYY161 *atg1Δ::URA3*	This study
YTS150	SEY6210 *ATG9-YFP::HIS5 atg1Δ::URA3 atg11Δ::LEU2*	Shintani and Klionsky, 2004b
YTS158	BY4742 *pho8::pho8Δ60 pho13Δ::KAN*	This study

was introduced into the pAPG9GFP(416) plasmid by site-directed mutagenesis. The Atg9 N-terminal region containing the AvrII site was amplified and introduced into pGBDU-C1 with EcoRI and BamHI to generate pBD-Atg9N(AvrII). A gapped pGBDU-C1 plasmid was generated by digesting with EcoRI and BamHI. The PCR reaction was performed using Taq polymerase (New England Biolabs, Inc.) with pBD-Atg9N(AvrII) as the template. The dATP concentration was lowered to three fifths that of the other three deoxynucleoside triphosphates. The resulting mutagenized PCR product shares overlapping sequences of ~100 bp at both 5′ and 3′ ends with the gapped pGBDU-C1 plasmid. The PCR product and the gapped plasmid were cotransformed into the two-hybrid strain PJ69-4A. The transformants were replicated on both −His and −Ade plates. The transformants that were not able to grow on either plate were selected and analyzed by Western blotting for protein stability using anti-Atg9 antiserum (Noda et al., 2000). Stable mutants were sequenced, and pBD-Atg9N^{H192L} was identified. The Atg9 N-terminal fragment containing the H192L mutation was then released from pBD-Atg9N^{H192L} by digestion at the introduced AvrII site and a natural NruI site. This fragment was cloned into pAPG9GFP(416) digested with the same restriction enzymes to generate pAtg9^{H192L}GFP(416).

Fluorescence microscopy

Cells expressing fusion proteins with fluorescence tags were grown in SMD media to OD_{600} = 0.8. For vacuolar membrane labeling, cells were pelleted, resuspended in fresh media at OD_{600} = 1.0, incubated with 2 μM FM 4-64 at 30°C for 15 min, and pelleted and cultured in the same media without FM 4-64 at 30°C for 30 min. For mitochondrial fluorescent labeling, MitoFluor red 589 (Invitrogen) was added to the growing culture at a final concentration of 1 μM, and the culture was incubated at 30°C for 30 min. Cells were then washed with the same culture medium before imaging to remove the excess dye. For rapamycin treatment, cells were cultured with 0.2 μg/ml rapamycin at 30°C for 1.5 h. When necessary, a mild fixation procedure was applied to visualize Atg9 without destroying various fluorescent proteins: cells were harvested, resuspended in a half volume of fixation buffer (50 mM KH_2PO_4, pH 8.0, 1.5% formaldehyde, and 1 μM $MgCl_2$), and incubated at room temperature for 30 min with gentle shaking. Cells were then washed once with an equal amount of wash buffer (50 mM potassium phosphate, pH 8.0, and 1 μM $MgCl_2$) and resuspended in 50 μl of wash buffer. Fluorescence signals were visualized on a fluorescence microscope (IX71; Olympus). The images were captured by a camera (Photometrics CoolSNAP HQ; Roper Scientific) and deconvolved using DeltaVision software (Applied Precision).

Additional assays

The GFP-Atg8 processing assay, the Pho8Δ60 activity assay, and the protease protection assay were performed as previously described (Noda et al., 1995; Wang et al., 2001; Abeliovich et al., 2003; Shintani and Klionsky, 2004b; Cheong et al., 2005).

The authors thank Dr. Weibin Zhou and members of the Klionsky laboratory for comments and suggestions.

D.J. Klionsky is supported by National Institutes of Health Public Health Service grant GM53396.

Submitted: 16 June 2006
Accepted: 16 November 2006

References

Abeliovich, H., C. Zhang, W.A. Dunn Jr., K.M. Shokat, and D.J. Klionsky. 2003. Chemical genetic analysis of Apg1 reveals a non-kinase role in the induction of autophagy. *Mol. Biol. Cell*. 14:477–490.

Cheong, H., T. Yorimitsu, F. Reggiori, J.E. Legakis, C.-W. Wang, and D.J. Klionsky. 2005. Atg17 regulates the magnitude of the autophagic response. *Mol. Biol. Cell*. 16:3438–3453.

Drubin, D.G., H.D. Jones, and K.F. Wertman. 1993. Actin structure and function: roles in mitochondrial organization and morphogenesis in budding yeast and identification of the phalloidin-binding site. *Mol. Biol. Cell*. 4:1277–1294.

Gerhardt, B., T.J. Kordas, C.M. Thompson, P. Patel, and T. Vida. 1998. The vesicle transport protein Vps33p is an ATP-binding protein that localizes to the cytosol in an energy-dependent manner. *J. Biol. Chem.* 273:15818–15829.

Huang, W.-P., S.V. Scott, J. Kim, and D.J. Klionsky. 2000. The itinerary of a vesicle component, Aut7p/Cvt5p, terminates in the yeast vacuole via the autophagy/Cvt pathways. *J. Biol. Chem.* 275:5845–5851.

Hutchins, M.U., M. Veenhuis and D.J. Klionsky. 1999. Peroxisome degradation in *Saccharomyces cerevisiae* is dependent on machinery of macroautophagy and the Cvt pathway. *J. Cell Sci*. 112:4079–4087.

James, P., J. Halladay, and E.A. Craig. 1996. Genomic libraries and a host strain designed for highly efficient two-hybrid selection in yeast. *Genetics*. 144:1425–1436.

Kamada, Y., T. Funakoshi, T. Shintani, K. Nagano, M. Ohsumi, and Y. Ohsumi. 2000. Tor-mediated induction of autophagy via an Apg1 protein kinase complex. *J. Cell Biol.* 150:1507–1513.

Kim, J., Y. Kamada, P.E. Stromhaug, J. Guan, A. Hefner-Gravink, M. Baba, S.V. Scott, Y. Ohsumi, W.A. Dunn Jr., and D.J. Klionsky. 2001. Cvt9/Gsa9 functions in sequestering selective cytosolic cargo destined for the vacuole. *J. Cell Biol.* 153:381–396.

Kim, J., W.-P. Huang, P.E. Stromhaug, and D.J. Klionsky. 2002. Convergence of multiple autophagy and cytoplasm to vacuole targeting components to a perivacuolar membrane compartment prior to de novo vesicle formation. *J. Biol. Chem.* 277:763–773.

Kirisako, T., M. Baba, N. Ishihara, K. Miyazawa, M. Ohsumi, T. Yoshimori, T. Noda, and Y. Ohsumi. 1999. Formation process of autophagosome is traced with Apg8/Aut7p in yeast. *J. Cell Biol.* 147:435–446.

Kirisako, T., Y. Ichimura, H. Okada, Y. Kabeya, N. Mizushima, T. Yoshimori, M. Ohsumi, T. Takao, T. Noda, and Y. Ohsumi. 2000. The reversible modification regulates the membrane-binding state of Apg8/Aut7 essential for autophagy and the cytoplasm to vacuole targeting pathway. *J. Cell Biol.* 151:263–276.

Klionsky, D.J. 2005. The molecular machinery of autophagy: unanswered questions. *J. Cell Sci.* 118:7–18.

Levine, B., and D.J. Klionsky. 2004. Development by self-digestion: molecular mechanisms and biological functions of autophagy. *Dev. Cell*. 6:463–477.

Longtine, M.S., A. McKenzie III, D.J. Demarini, N.G. Shah, A. Wach, A. Brachat, P. Philippsen, and J.R. Pringle. 1998. Additional modules for versatile and economical PCR-based gene deletion and modification in *Saccharomyces cerevisiae. Yeast*. 14:953–961.

Monastyrska, I., T. Shintani, D.J. Klionsky, and F. Reggiori. 2006. Atg11 directs autophagosome cargoes to the PAS along actin cables. *Autophagy*. 2:119–121.

Nair, U., and D.J. Klionsky. 2005. Molecular mechanisms and regulation of specific and nonspecific autophagy pathways in yeast. *J. Biol. Chem.* 280:41785–41788.

Noda, T., A. Matsuura, Y. Wada, and Y. Ohsumi. 1995. Novel system for monitoring autophagy in the yeast *Saccharomyces cerevisiae*. *Biochem. Biophys. Res. Commun.* 210:126–132.

Noda, T., J. Kim, W.-P. Huang, M. Baba, C. Tokunaga, Y. Ohsumi, and D.J. Klionsky. 2000. Apg9p/Cvt7p is an integral membrane protein required for transport vesicle formation in the Cvt and autophagy pathways. *J. Cell Biol.* 148:465–480.

Noda, T., K. Suzuki, and Y. Ohsumi. 2002. Yeast autophagosomes: de novo formation of a membrane structure. *Trends Cell Biol.* 12:231–235.

Oda, M.N., S.V. Scott, A. Hefner-Gravink, A.D. Caffarelli, and D.J. Klionsky. 1996. Identification of a cytoplasm to vacuole targeting determinant in aminopeptidase I. *J. Cell Biol.* 132:999–1010.

Reggiori, F., and D.J. Klionsky. 2005. Autophagosomes: biogenesis from scratch? *Curr. Opin. Cell Biol.* 17:415–422.

Reggiori, F., K.A. Tucker, P.E. Stromhaug, and D.J. Klionsky. 2004. The Atg1-Atg13 complex regulates Atg9 and Atg23 retrieval transport from the pre-autophagosomal structure. *Dev. Cell*. 6:79–90.

Reggiori, F., I. Monastyrska, T. Shintani, and D.J. Klionsky. 2005a. The actin cytoskeleton is required for selective types of autophagy, but not nonspecific autophagy, in the yeast *Saccharomyces cerevisiae*. *Mol. Biol. Cell*. 16:5843–5856.

Reggiori, F., T. Shintani, U. Nair, and D.J. Klionsky. 2005b. Atg9 cycles between mitochondria and the pre-autophagosomal structure in yeasts. *Autophagy*. 1:101–109.

Robinson, J.S., D.J. Klionsky, L.M. Banta, and S.D. Emr. 1988. Protein sorting in *Saccharomyces cerevisiae*: isolation of mutants defective in the delivery and processing of multiple vacuolar hydrolases. *Mol. Cell. Biol.* 8:4936–4948.

Scott, S.V., A. Hefner-Gravink, K.A. Morano, T. Noda, Y. Ohsumi, and D.J. Klionsky. 1996. Cytoplasm-to-vacuole targeting and autophagy employ the same machinery to deliver proteins to the yeast vacuole. *Proc. Natl. Acad. Sci. USA*. 93:12304–12308.

Shintani, T., and D.J. Klionsky. 2004a. Autophagy in health and disease: a double-edged sword. *Science*. 306:990–995.

Shintani, T., and D.J. Klionsky. 2004b. Cargo proteins facilitate the formation of transport vesicles in the cytoplasm to vacuole targeting pathway. *J. Biol. Chem.* 279:29889–29894.

Shintani, T., W.-P. Huang, P.E. Stromhaug, and D.J. Klionsky. 2002. Mechanism of cargo selection in the cytoplasm to vacuole targeting pathway. *Dev. Cell*. 3:825–837.

Tucker, K.A., F. Reggiori, W.A. Dunn Jr., and D.J. Klionsky. 2003. Atg23 is essential for the cytoplasm to vacuole targeting pathway and efficient autophagy but not pexophagy. *J. Biol. Chem*. 278:48445–48452.

Wang, C.-W., J. Kim, W.-P. Huang, H. Abeliovich, P.E. Stromhaug, W.A. Dunn Jr., and D.J. Klionsky. 2001. Apg2 is a novel protein required for the cytoplasm to vacuole targeting, autophagy, and pexophagy pathways. *J. Biol. Chem.* 276:30442–30451.

Yen, W.-L., J.E. Legakis, U. Nair, and D.J. Klionsky. 2006. Atg27 is required for autophagy-dependent cycling of Atg9. *Mol. Biol. Cell.* In press.

Yorimitsu, T., and D.J. Klionsky. 2005. Atg11 links cargo to the vesicle-forming machinery in the cytoplasm to vacuole targeting pathway. *Mol. Biol. Cell*. 16:1593–1605.

Young, A.R.J., E.Y.W. Chan, X.W. Hu, R. Köchl, S.G. Crawshaw, S. High, D.W. Hailey, J. Lippincott-Schwartz, and S.A. Tooze. 2006. Starvation and ULK1-dependent cycling of mammalian Atg9 between the TGN and endosomes. *J. Cell Sci.* 119:3888–3900.